Effect of implanted species on thermal evolution of ion-induced defects in ZnO

A. Yu. Azarov,[1] A. Hallén,[2] X. L. Du,[3] P. Rauwel,[1] A. Yu. Kuznetsov,[1] and B. G. Svensson[1]
[1]*Department of Physics, Centre for Materials Science and Nanotechnology, University of Oslo, PO Box 1048 Blindern, N-0316 Oslo, Norway*
[2]*Royal Institute of Technology, KTH-ICT, Electrum 229, SE-164 40, Kista, Stockholm, Sweden*
[3]*Institute of Physics, The Chinese Academy of Sciences, Beijing 100190, China*

(Received 2 January 2014; accepted 5 February 2014; published online 21 February 2014)

Implanted atoms can affect the evolution of ion-induced defects in radiation hard materials exhibiting a high dynamic annealing and these processes are poorly understood. Here, we study the thermal evolution of structural defects in wurtzite ZnO samples implanted at room temperature with a wide range of ion species (from ^{11}B to ^{209}Bi) to ion doses up to 2×10^{16} cm^{-2}. The structural disorder was characterized by a combination of Rutherford backscattering spectrometry, nuclear reaction analysis, and transmission electron microscopy, while secondary ion mass spectrometry was used to monitor the behavior of both the implanted elements and residual impurities, such as Li. The results show that the damage formation and its thermal evolution strongly depend on the ion species. In particular, for F implanted samples, a strong out-diffusion of the implanted ions results in an efficient crystal recovery already at 600 °C, while co-implantation with B (via BF_2) ions suppresses both the F out-diffusion and the lattice recovery at such low temperatures. The damage produced by heavy ions (such as Cd, Au, and Bi) exhibits a two-stage annealing behavior where efficient removal of point defects and small defect clusters occurs at temperatures ~500 °C, while the second stage is characterized by a gradual and partial annealing of extended defects. These defects can persist even after treatment at 900 °C. In contrast, the defects produced by light and medium mass ions (O, B, and Zn) exhibit a more gradual annealing with increasing temperature without distinct stages. In addition, effects of the implanted species may lead to a nontrivial defect evolution during the annealing, with N, Ag, and Er as prime examples. In general, the obtained results are interpreted in terms of formation of different dopant-defect complexes and their thermal stability. © *2014 AIP Publishing LLC*.
[http://dx.doi.org/10.1063/1.4866055]

I. INTRODUCTION

ZnO is one of the most extensively studied materials during the past decade due to its remarkable properties and potential technological importance which is difficult to overestimate (see, for example, the reviews[1,2] and references therein). Indeed, ZnO with its direct wide band-gap ($E_g \approx 3.4$ eV) and high exciton binding energy (≈60 meV) is a promising candidate for a number of optoelectronic devices. Furthermore, ZnO can be used as a dilute magnetic semiconductor (DMS) having its Curie temperature above room temperature.[3] In addition to availability of large area bulk single crystals, ZnO can be grown in a variety of nanostructured morphologies by low cost and low temperature methods.[4] Doping with desirable impurities is a key process in the fabrication of devices, and ion implantation, among other doping techniques, provides a possibility to introduce controllable amounts of impurities at precise depth/areas of a sample, not limited by the equilibrium solubility.

It has previously been shown that ZnO exhibits a strong degree of dynamic annealing during ion bombardment,[5,6] which means that ion-induced intrinsic defects, i.e., Zn/O interstitials and vacancies, to a very large extent recombine during the ion beam exposure. Such strong dynamic annealing processes lead to an extreme radiation hardness and ZnO remains crystalline even upon implantations with high doses at low temperatures, where each lattice atom is on average displaced up to hundred times.[5,7] However, the dynamic annealing is not 100% efficient and various types of residual defects, including clusters and extended stacking faults, accumulate during the ion bombardment.[8,9] Such defects are often detrimental for device performance and, therefore, a number of recent ZnO studies have focused on minimization/removal of ion-induced defects.[10–20] For instance, implantation along one of the main channeling directions results in considerably lower damage production compared with that for a random one.[10] However, channeling implantation usually leads to a significant broadening of the dopant distribution and, hence, it is not suitable for the formation of shallow and well-controlled dopant profiles. Recently, it has been shown that enhanced defect annihilation at interfaces can be potentially explored for the suppression of damage accumulation in non-metallic solids.[11,12] Also, implantation at elevated temperatures may have a positive impact on dopant activation due to enhanced dynamic annealing.[13] Alternatively, post-implantation annealing can be used to remove ion-induced defects.[14–20] However, despite rather intensive efforts during the past decade, the processes of defect evolution during post-implantation annealing of ZnO are far from being fully understood.

 © 2014 AIP Publishing LLC

The data available in the literature are somewhat contradictory, but, it can be concluded that a substantial removal of irradiation-induced defects occurs at temperatures of 600–1200 °C.[14–17] Already in 1988, Sonder *et al.*[15] showed that the temperature at which defects disappear is related to the implanted species, but no apparent correlation between this defect annealing and out-diffusion of the implanted species was found. On the other hand, for rare earth implants, it has been suggested that the lattice recrystallization drives out the implanted species,[10,16] which can be attributed to the low solubility of rare earth elements in ZnO. Depending on the implanted species, a strong vacancy clustering can occur in the low temperature range of 200–600 °C as measured by positron annihilation spectroscopy (PAS).[17,18] Such clustering can lead to the formation of microvoids, which require much higher temperatures to disappear.[17] It should be noted that annealing conditions are sometimes limited by the tendency of ZnO to loose oxygen from the surface and decompose[19] above 1000 °C, and these processes can be stimulated by implantation-induced defects[20] to occur even below 1000 °C.

It has previously been shown that disorder accumulation in ZnO exhibits a four-stage behavior with ion dose:[21] (i) low dose regime with linear damage growth, (ii) a first saturation of the relative damage concentration at a value of ~2%, (iii) a second increase in the damage concentration, and (iv) a second plateau at about 50%. The third stage is characterized by a rapid damage growth occurring between the two saturation plateaus for a dose range corresponding to 1–15 displacements per atom (DPA).[22] The variation of such implantation parameters as ion flux and cascade density has a small effect on the damage formation[6,28] in this third stage, indicating predominantly linear defect interaction and, therefore, the role of implanted atoms in the defect formation cannot be excluded. In this study, we report on a comprehensive and systematic investigation of the influence of the ion species (ranging from ^{11}B to ^{209}Bi) on the thermal stability of ion-induced defects in c-oriented wurtzite ZnO samples implanted to relatively high ion doses (DPA > 1). Moreover, as recently shown,[23] the evolution of self-interstitials (Zn_i and O_i) in ZnO can be traced by monitoring of Li, which is one of the main electrically active and residual impurities in hydrothermally (HT) grown ZnO. Thus, in addition to follow the development of structural disorder and dopant behavior, also the evolution of Li was studied. We demonstrate that dopant-defect interaction and dopant stability play a key role in the thermal evolution of irradiation-induced defects in monocrystalline ZnO.

II. EXPERIMENTAL

HT grown and molecular beam epitaxy (MBE) grown wurtzite ZnO wafers were implanted at room temperature with 11 different kinds of ions ranging from ^{11}B to ^{209}Bi (see Table I which summarizes the implantation parameters used). Note that energies and doses for O/Zn and N/B/BF_2 ions were selected such that similar defect generation profiles as well as total number of primary defects were obtained for each group of implants, as estimated by Monte Carlo simulations using the TRIM code.[25] All the implantations were carried out at 7° off the [0001] direction in order to reduce channeling. After implantation, the samples were annealed at temperatures in the range of 400–1050 °C for 30–60 min in air.

The ion-induced structural disorder was analyzed by Rutherford backscattering spectrometry in the channeling mode (RBS/C) with 2 MeV ^{4}He$^+$ ions backscattered into detectors placed at 100° and 170° relative to the incident beam direction. The so-called glancing-angle detector geometry (100°) was used to provide enhanced depth resolution, specifically in the near-surface region, while the 170° geometry was used to provide enhanced mass resolution to carefully examine the configurations of the implanted heavy species. The fraction of atoms occupying substitutional positions was calculated by comparing the RBS spectra obtained under channeling and random conditions. The RBS/C spectra were also analyzed with a well-established algorithm[26] to deduce an effective number of so-called scattering centers. The calculated number of scattering centers normalized to the atomic concentration is referred to below as "relative disorder," whose magnitude varies from zero to unity corresponding to a "defect-free" and an amorphous state, respectively. It should be noted that determination of disorder levels on the oxygen sublattice using the RBS/C

TABLE I. Implant parameters used in this study. Also given are the calculated values of DPA[22] and projected ranges of implanted ions (R_p). The average densities of individual collision cascades (f_{dm}) were calculated at the depth of maximum of the nuclear energy loss profiles (R_{pd}) using a recently developed algorithm.[24]

Sample	Ion	Energy (keV)	Ion flux (cm^{-2} s^{-1})	Dose (cm^{-2})	DPA	R_p (nm)	R_{pd} (nm)	f_{dm} (at. %)
MBE	^{16}O	35	6×10^{12}	2×10^{16}	10.5	54	32	0.06
MBE	^{64}Zn	150	3×10^{11}	4×10^{15}	10.5	58	37	0.15
HT	^{11}B	35	3.8×10^{12}	1.5×10^{16}	4	90	55	0.02
HT	^{15}N	50	1.9×10^{13}	1×10^{16}–3×10^{16}	4–12	90	55	0.04
HT	^{19}F	50	6.3×10^{12}	2×10^{16}	12	55	40	0.055
HT	$^{49}BF_2$	155	6.3×10^{12}	3×10^{15}	4	90	55	0.04
HT	^{107}Ag	500	1×10^{11}	5×10^{15}	20.5	120	86	0.085
HT	^{112}Cd	250	8×10^{12}	$5 \times 10^{14} - 5 \times 10^{15}$	2.2–22	60	40	0.2
HT	^{166}Er	200	4×10^{12}	1.5×10^{15}	8.7	40	27	0.4
HT	^{197}Au	200	1×10^{12}	5×10^{15}	32	35	23	0.45
HT	^{209}Bi	270	6.3×10^{12}	1×10^{16}	69	45	28	0.33

technique is difficult due to large difference in atomic masses between O and Zn. Therefore, in addition to RBS/C, high energy experiments were performed to reach the region of non-Rutherford scattering cross section to enhance the yield from displaced oxygen atoms. For this purpose, $^{16}O(\alpha, \alpha)^{16}O$ nuclear reaction analysis in channeling mode (NRA/C)[27] was carried out at the scattering angle of 170°. The resonance is centered around 3.045 MeV and has an enhanced cross section with a factor of 17 compared with the regular Rutherford cross section. The relative damage on the oxygen sublattice was calculated from the NRA/C spectra as $(\chi_{ch} - \chi_v)/(\chi_r - \chi_v)$, where χ_{ch} and χ_v are the maximum resonant peak values in channeling spectra for the implanted and virgin samples, respectively, while χ_r is the corresponding random value at the same depth.

Despite the possibility to draw at least qualitative conclusions on the type of defects observed, using RBS/C only, identification of defect microstructure by ion channeling techniques is challenging. Therefore, transmission electron microscopy (TEM) was also employed to characterize the defect microstructure in some selected samples. Specimens for TEM were prepared by mechanical thinning followed by 4 keV Ar-ion milling for approximately 30 min at room temperature. Characterization was carried out along the ⟨11–20⟩ zone axis using a JEM2010F microscope operating at 200 kV and disposing a point to point resolution of 1.9 Å.

Concentration versus depth profiles of Li as well as of the light mass elements B, N, and F were measured by secondary ion mass spectrometry (SIMS) using a Cameca IMS 7f microanalyzer with 10 keV O_2^+ or 15 keV Cs^+ ions as primary beam for the analysis. The intensity-concentration calibration was performed using as-implanted samples as references. Depth conversion of the profiles was performed by measuring the sputtered crater depth using a Dektak 8 stylus profilometer and assuming a constant erosion rate.

III. RESULTS AND DISCUSSION

A. Implantation with self-ions

Fig. 1 illustrates the damage evolution in MBE grown samples implanted with self-ions (O and Zn) to doses resulting in the same DPA value of 10.5 (see Table I for further details). Both implants produce nearly the same amount of damage in the region of the projected range (R_p) despite the difference in average collision cascade density. This result is consistent with previous experimental observations where it has been shown that the disorder at the maximum of its distribution does not hinge on the collision cascade density and can be predicted by ballistic calculations using a linear approximation in the range of 0.5–15 DPA.[28] However, the shape of the damage distributions caused by Zn and O ions as well as their thermal evolution is quite different. The O implantation results in the formation of a strong bulk damage peak close to R_p (Fig. 1(a)), while the Zn ions give rise to a broad disorder profile with pronounced damage near the surface and a relatively high dechanneling tail behind the damage peak (Fig. 1(b)). Such an enhanced yield of the dechanneling tails in RBS/C spectra is usually attributed to the formation of extended defects, e.g., dislocation loops

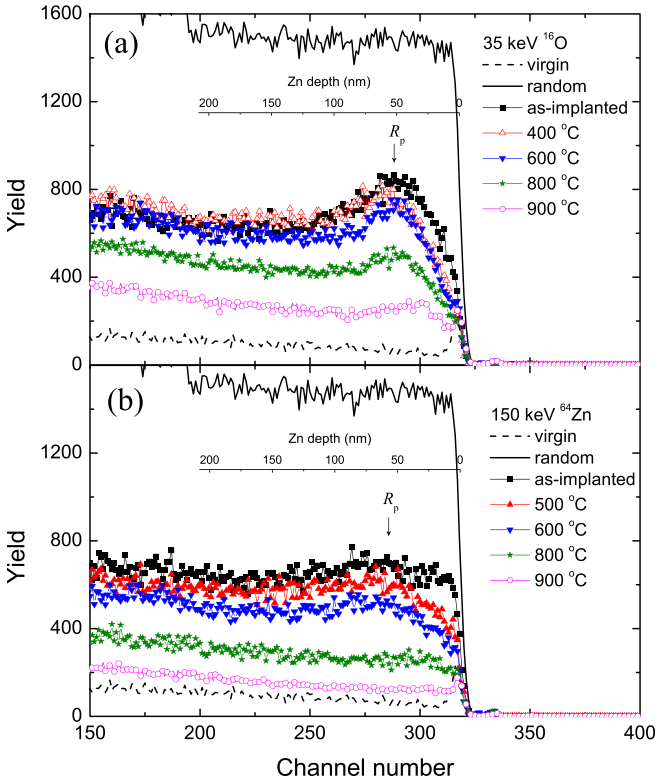

FIG. 1. RBS/C spectra (acquired with 100° detector geometry) of MBE-ZnO implanted with (a) 35 keV $^{16}O^+$ ions to 2×10^{16} cm^{-2} and (b) 150 keV $^{64}Zn^+$ ions to 4×10^{15} cm^{-2} before and after annealing as indicated in the legend. The channeling spectra of unprocessed (virgin) samples are also shown for comparison by the dashed lines. The projected ranges of the implanted ions (R_p), predicted by TRIM code[25] simulations are depicted in the panels relative to the Zn depth scale.

and/or stacking faults,[29] which do not contribute to direct backscattering of the analyzing ions. Thus, the nature of the damage produced by the O and Zn ions is quite different but this is attributed to the role of the excess of O or Zn atoms introduced rather than difference in the collision cascade densities, as will be further discussed for the case of heavy ions in Sec. III F.

It is suggested that the implanted Zn atoms contribute to the growth of extended defects of interstitial type, while the O atoms primarily form O_i-related complexes of small size. Such a suggestion is also corroborated by a lower activation energy for Zn_i diffusion compared with that for O_i,[30] despite that the actual diffusivity of primary (intrinsic) defects can be considerably higher during ion bombardment than equilibrium values due to ionization-enhanced motion.[31] Furthermore, Fig. 1(a) reveals that annealing of the Zn implanted samples leads to a gradual loss of the extended defects and after 900 °C, the crystal restoration is almost complete. However, for O, a considerable amount of the damage still remains after 900 °C and the crystal recovery is limited.

B. Implantation with light ions

The thermal evolution of damage in HT-samples bombarded with light ions is illustrated by Fig. 2 showing RBS/C spectra for (a) B, (b) N, and (c) F implants before and after

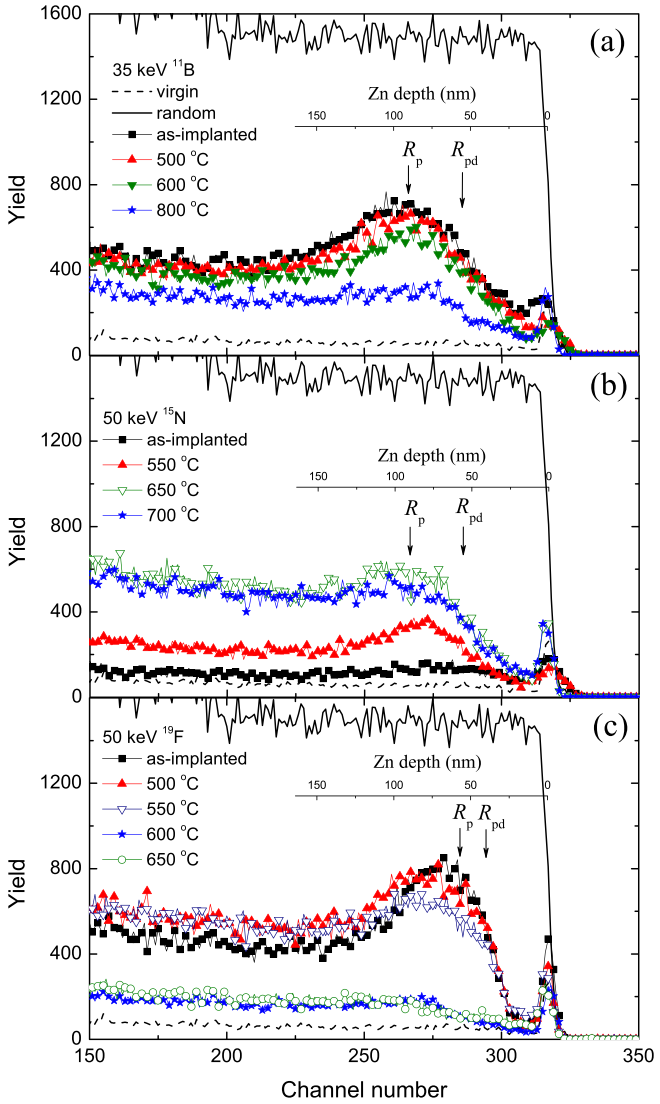

FIG. 2. RBS/C spectra (acquired with 100° detector geometry) of HT-ZnO implanted with (a) 35 keV $^{11}B^+$ ions to 1.5×10^{16} cm^{-2}, (b) 50 keV $^{14}N^+$ ions to 1×10^{16} cm^{-2}, and (c) 50 keV $^{19}F^+$ ions to 2×10^{16} cm^{-2} before and after annealing as indicated in the legend. The channeling spectra of unprocessed (virgin) samples are shown for comparison by the dashed lines. The projected ranges of the implanted ions (R_p) and maximum of the nuclear energy loss profiles (R_{pd}), predicted by TRIM code[25] simulations are depicted in the panels relative to the Zn depth scale.

annealing. The damage build-up and its thermal evolution are dramatically different for these three kinds of ions. In particular, for B, the damage peak exhibits a gradual decrease similar to that for O (see Sec. III A), while for N, a reverse annealing takes place with increasing temperature, reaching a maximum disorder at ~650 °C. In contrast, the damage induced by F ions exhibits a weak reduction up to 550 °C, whilst a further increase by only 50 °C leads to an almost complete recovery of the crystal lattice. These effects are quantitatively illustrated in Fig. 3 showing the maximum relative disorder as a function of annealing temperature for the three ions. The damage produced by F ions displays lower thermal stability as compared with that for the other two and this can be directly attributed to the out-diffusion of F. The inset in Fig. 3 shows the retained dose of F ions in the implantation peak region after annealing, and the almost full

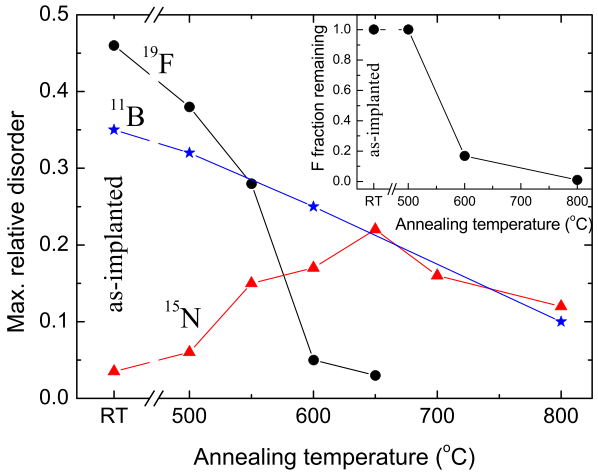

FIG. 3. Relative disorder on the Zn-sublattice as deduced from the maximum of the damage profiles in the crystal bulk of ZnO as a function of annealing temperature after ^{11}B (stars), ^{15}N (triangles), and ^{19}F (circles) implants. The inset shows the fraction of retained F dose in the implanted region as a function of annealing temperature.

crystal recovery at 600 °C is accompanied by a dramatic loss of F, as also corroborated by the recent results in Ref. 32. Such a strong correlation between the damage stability and that of the implanted species indicates a key role of the latter for the thermal evolution of ion-induced defects in ZnO.

For B, an anomalously high damage generation occurs compared with that for N, despite similar DPA values (equal to 4) and also positions and shapes of the primary defect distributions deviate from those estimated by TRIM code[25] simulations. Furthermore, ballistic calculations combined with an empirical formula to account for dynamic annealing[28] predict a maximum relative damage in the bulk peak of $\sim 0.12 \pm 0.03$ for DPA = 4. This value is considerably lower than that found for B (~0.35) and higher than that for N (~0.04). Such a strong damage enhancement for B can be attributed to formation of B-O complexes and boron clustering which is likely to take place at the high dose used (1.5×10^{16} cm^{-2}). Similar effects resulting in an enhanced damage accumulation have been observed previously in other semiconductors; for instance, in Si bombarded with C ions at room temperature where the effect was attributed to the formation of stable complexes between Si self-interstitials and C atoms.[33] Moreover, impurity stabilization of intrinsic defects has been put forward to explain enhanced damage formation leading to amorphization of ZnO during implantation with high doses of Si.[5] The disorder evolution in the N implanted samples exhibits an exceptional behavior with temperature and is discussed in detail in Sec. III C.

C. Defect stability and reverse annealing in N implanted samples

As shown in Sec. III B, N implantation results in a lower damage production compared with that for the other ions at the ion dose resulting in 4 DPA.[34] However, increasing the N dose from 1×10^{16} to 3×10^{16} cm^{-2} yields a fast damage growth reaching ~50% for 12 DPA (3×10^{16} cm^{-2}) as clearly illustrated by Fig. 4, where also the thermal evolution

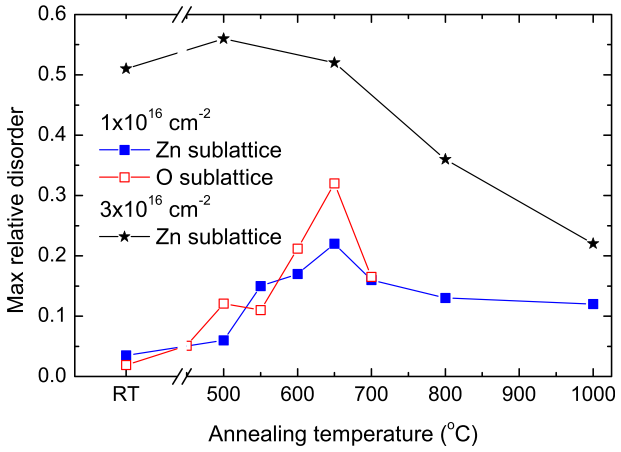

FIG. 4. Relative disorder on the Zn- (closed symbols) and O-sublattice (open symbols) in the crystal bulk of ZnO as a function of annealing temperature after ^{15}N implantations with two different doses as indicated in the legend.

of disorder on the separate Zn- and O-sublattices is shown. The observed sharp dose dependence of damage accumulation for N ions reflects a strong nonlinearity of defect formation at the third stage of damage accumulation and it is likely due to formation of N related defect complexes. Indeed, it has been shown that the damage accumulation in ZnO exhibits a IV-stage behavior as a function of dose and the obtained value of relative disorder in the as-implanted state for N ($\sim$0.04) is close to that of the first saturation stage.[7] In Ref. 7, it has been suggested that the first saturation stage is related to instability of large defect clusters while further growth at higher doses is due to the pronounced role of the implanted species in damage stabilization. The key role of the implanted N ions in the formation of nucleation sites for damage growth is also indirectly supported by the fact that the damage peak position in the low dose (1×10^{16} N/cm^2) as-implanted sample is located close to maximum of the nuclear energy loss profiles (R_{pd}) (Fig. 2(b)), in strong contrast to that for high dose (3×10^{16} N/cm^2) where the damage peak position coincides with R_p (not shown). Therefore, the low dose corresponds to the transition region between second and third stages where disorder accumulation is still mainly determined by ballistic processes but the concentration of implanted atoms starts to become relatively high and affect the processes of dynamic annealing.

The reverse annealing observed in the N implanted samples is intriguing. Reverse annealing has previously been observed in different semiconductors, such as Si[35,36] and Ge[37] implanted with large doses of H ions. However, even for these materials, the mechanisms of reverse annealing are not fully understood and it has been speculated that formation and evolution of H_2 filled cavities or platelets can play a role.[36] In ZnO samples implanted with N (Ref. 18) and B ions,[17] open volume defects on the Zn sublattice, studied by PAS, start to cluster and grow in size upon annealing in the temperature range of 300–600 °C. This holds for both N and B, while our data reveal completely different behaviors of the displaced Zn atoms (interstitial type defects) for the two types of ions (see Figs. 2 and 3).[38] Therefore, the reverse annealing in the N implanted samples cannot be immediately ascribed as a counter part to the clustering of Zn vacancies, and "chemical" effects of the N atoms should be considered. Indeed, N is frequently considered as a promising element for *p*-type doping of ZnO, although its properties as shallow acceptor and the reproducibility of *p*-type conduction are challenged by deep acceptor states of N substituting on O-site and compensation effects of N-related defect complexes.[39,40] For instance, the formation of molecular nitrogen N_2 substituting on O site is possible for temperatures above 470 °C,[39] which is close to the temperature range where the reverse annealing takes place. This is also corroborated by the minor reverse annealing in the high dose sample since a probability of N clustering already in as-implanted state should increase with ion dose. Here, it should be pointed out that the disorder on the O-sublattice shows a similar evolution with annealing temperature as that on the Zn-sublattice, according to the NRA/C data depicted in Fig. 4 by open symbols.[41] Moreover, the crucial role of the N atoms for the defect evolution is also corroborated by the distinct shift of the damage peak position from R_{pd} to R_p during the reverse annealing, as clearly illustrated by Fig. 2(b). In contrast to the low dose (sample 1×10^{16} N/cm^2), the disorder in the sample implanted to 3×10^{16} N/cm^2 exhibits neither a strong reverse annealing (Fig. 4) nor a shift of the damage peak position, which agrees well with R_p already in the as-implanted state (not shown).

Additionally, it should be mentioned that irrespective of the N dose used, the disorder has an exceptionally high thermal stability and a significant damage fraction still persists even after annealing at 1000 °C. A high thermal stability of vacancy clusters in N doped ZnO has been reported also by Tuomisto *et al.*[42] Such stabilization was observed independently on the N doping technique used and it was suggested that strain-induced effects caused by N incorporation on O-sites play a decisive role in the formation of the stable vacancy clusters.[42] However, further work needs to be pursued for a better understanding of both the damage formation and annealing effects in N implanted samples.

D. Li evolution in HT-samples implanted with light ions

In contrast to heavy element implants, the RBS signal from light implanted ions is typically very low, hidden by a strong background from the matrix elements, which makes an analysis of the lattice location of the element difficult based on RBS/C data. However, information on atomic configurations and defect behavior in ZnO can be obtained by monitoring the evolution of Li concentration versus depth profiles;[23] Li is a common residual impurity in HT-ZnO with typical concentration in the range of $\sim 10^{17}$ cm^{-3}. Figs. 5(a), 5(b), and 6 summarize the results on Li evolution in the N, F, and B implanted samples, respectively, as measured with SIMS. The Li redistribution is drastically different for all the three types of implants. In particular, Li accumulates in the region around R_p for the N implanted sample after annealing at 600 °C (see Fig. 5(a)), while in the B implanted sample, it starts to redistribute already at 500 °C and exhibits an extremely wide Li-depleted layer reaching almost 30 μm

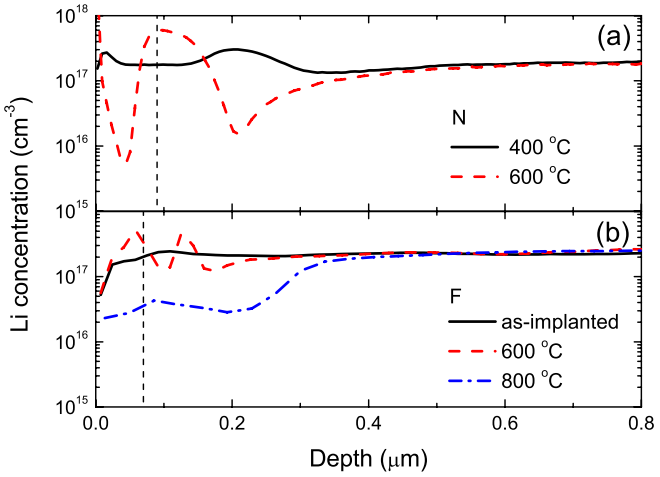

FIG. 5. Li concentration versus depth profiles as measured by SIMS in ZnO implanted with (a) 50 keV N^+ ions and (b) 50 keV F^+ ions before and after annealing as indicated in the legend. The vertical, dashed lines mark the projected ranges of the implanted ions.

after 800 °C (Fig. 6). Both N and B display a rather weak redistribution at temperatures up to 800 °C (not shown) and therefore, the dramatic difference in Li behavior is most likely associated with different changes of local atomic configuration of N and B during the annealing. It is known that Li preferentially occupies Zn sites (Li_{Zn}) in *n*-type material[43] and, as shown previously,[23] the strong Li depletion behind the implantation peak is typical for implantations with Zn-substituting elements and ascribed to fast moving interstitial Li, formed via the kick-out mechanism ($Zn_i + Li_{Zn} \rightarrow Zn_{Zn} + Li_i$). Hence, these data provide strong evidence that the B atoms occupy preferentially Zn sites during post-implant annealing, but not the N atoms. The Zn_is are presumably released from the B-implanted region via thermally-induced dissociation of complexes involving Zn_i, formed during the implantation. The efficiency of this mechanism can be roughly estimated by comparing the amounts of displaced Zn atoms and removed Li atoms from the depleted region. The results of such an analysis are depicted

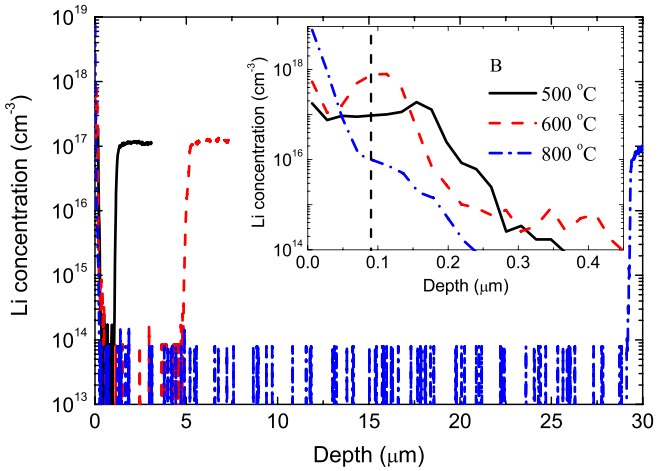

FIG. 6. Li concentration versus depth profiles as measured by SIMS in ZnO implanted with 35 keV B^+ ions before and after annealing as indicated in the legend. The inset shows the enlarged near the surface part of the profiles. The vertical, dashed line in the inset marks the projected range of the implanted ions.

in Fig. 7 showing the temperature dependencies of total amount of Li removed from the depleted region (left-hand scale) and the total number of displaced Zn atoms (scattering centers) in the damage peak as deduced from RBS/C data (right-hand scale). The amount of removed Li atoms is considerably lower than both the amount of displaced Zn atoms being annealed and the implanted B dose (1.5×10^{16} cm^{-2}). The ratio between the amount of removed Li atoms and the amount of displaced Zn atoms disappearing is in the range of ~0.001–0.003 with an increasing tendency as a function of annealing temperature.

In the region around R_p, the B and N implanted samples subjected to 600 °C anneals actually demonstrate rather similar behavior with respect to the Li redistribution (see Fig. 5(a) and the inset in Fig. 6). These data are consistent with previous studies of the Li evolution around R_p in N implanted samples[18] and also resemble those observed for O implanted samples.[23] As mentioned in Sec. III B, the temperature range around 600 °C is characterized by a strong evolution of open volume defects in B, O, and N implanted samples and the Li pile-up in the implantation peak region can be attributed to trapping of Li by these defects. In contrast, in the F implanted samples, Li exhibits only a weak redistribution around R_p during annealing at 600 °C (see Fig. 5(b)), indicating a modest vacancy clustering as compared with that for the B, N, and O implants.

E. Damage stabilization by co-implantation

As discussed in Sec. III B, the efficient lattice recovery at relatively low temperatures in the F implanted samples is attributed to the out-diffusion of F from the damaged region. However, Fig. 8 illustrates that the presence of B atoms in the damaged region after BF_2 implants can efficiently stabilize the ion-induced damage and suppress the F redistribution during post-implantation annealing. The data in Fig. 8 compare the relative crystal recovery and the loss of F as a function of annealing temperature for F and BF_2 implanted samples. The crystal recovery trends in the BF_2 samples are similar to those in the B implanted ones (see Fig. 2(a)), i.e.,

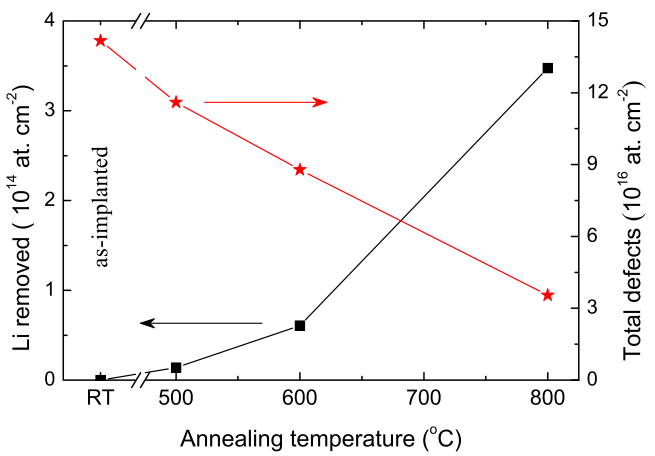

FIG. 7. Amount of Li removed from the depletion region as deduced from SIMS data (squares, left-hand scale) and total number of displaced Zn atoms (scattering centers) as deduced from RBS data (stars, right-hand scale) as a function of annealing temperature.

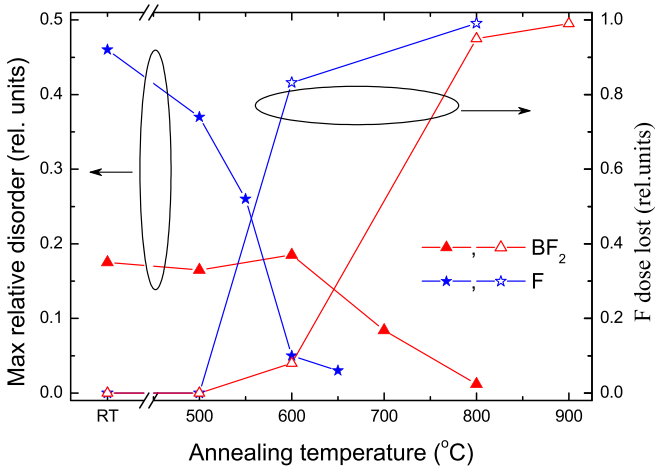

FIG. 8. Relative disorder on the Zn-sublattice as deduced from the maximum of the damage profiles in ZnO implanted with 50 keV F^+ ions to 2×10^{16} cm^{-2} and 155 keV BF_2 to 3×10^{15} cm^{-2} (left-hand scale, closed symbols) and the fraction of lost F dose in the implanted region (right-hand scale, open symbols) as a function of annealing temperature.

the temperature required for efficient lattice recovery is ~800 °C and considerably higher than that for the samples implanted with F ions only (~600 °C). Concurrently, also the F out-diffusion is retarded in the co-implanted samples, and similar to that in the F implanted samples, F starts to diffuse out from the implanted region at the same temperatures where efficient lattice recovery occurs.

The immobilization of F in the BF_2 co-implanted samples may suggest that O interstitials mediate the F diffusion; F is anticipated to be an O-substituting element and it is likely trapped by O sites, while B resides preferentially on Zn sites forming B-O complexes.[17] Therefore, the suppressed out-diffusion of F may be attributed to the formation of stable B-O complexes preventing a sufficient concentration of O_i to promote out-diffusion of F. In addition, also a direct B-F interaction resulting in formation of stable B-F_n complexes cannot be excluded.

F. Enhanced formation of extended defects after Ag implantation

The damage evolution in samples implanted with medium mass ions is illustrated in Fig. 9, showing RBS/C spectra after bombardment with (a) Cd and (b) Ag ions before and after annealing. The Cd ions produce a strong damage peak in the vicinity of R_p. However, in contrast to the low mass implants, the damage annealing in the Cd implanted samples exhibits a two-stage behavior, where the 500 °C treatment results in a strong reduction of the disorder, while further annealing at higher temperatures induces only a small crystal recovery (Fig. 9(a)). Moreover, all spectra of the annealed samples display an increased dechanneling yield in the end-of-range region, similar to that observed in the Zn implanted samples (see Sec. III A). Thus, efficient annealing of point defects and small defect clusters occurs during the first stage, while the second stage is dominated by extended defects which require higher temperatures to disappear. Such extended defects can be formed either directly during the implantation due to the high density of the collision cascades

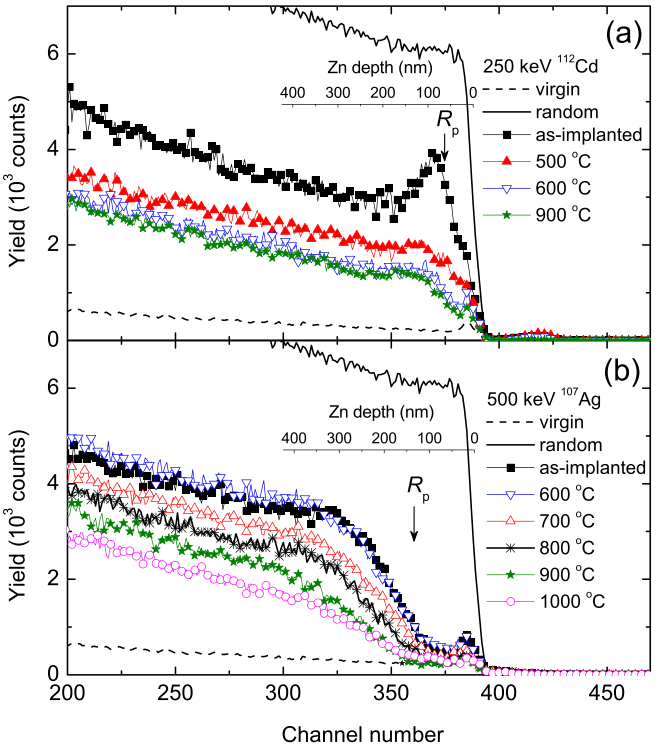

FIG. 9. RBS/C spectra (acquired with 170° detector geometry) of HT-ZnO implanted with (a) 250 keV $^{112}Cd^+$ ions and (b) 500 keV $^{107}Ag^+$ ions to 5×10^{15} cm^{-2} before and after annealing as indicated in the legends. The channeling spectra of unprocessed (virgin) samples are shown for comparison by the dashed lines. The projected ranges of the implanted ions (R_p), predicted by TRIM code[25] simulations are depicted in the panels relative to the Zn depth scale.

compared with that for light ions (see the Table I) or during the subsequent annealing. It should be noted that the efficient point defect annealing at low temperatures, compared with that for the light ion implants, may be attributed to the high concentration of extended defects which can be efficient annihilation sinks for mobile point defects.

Interestingly, despite that Cd and Ag have similar atomic masses, the defect formation/evolution in the samples implanted with these elements is considerably different. In contrast to Cd, the RBS/C spectra of the Ag implanted samples do not show a well defined damage peak, Fig. 9(b). Instead, its shape is characterized by an enhanced yield behind R_p of the Ag ions (marked by the arrow), while the part of the spectrum before R_p is close to that for the unimplanted sample. Damage annealing in the Ag implanted samples exhibits a single stage behavior where temperatures up to 600 °C have a minor effect, while annealing at higher temperatures leads to a gradual recovery of the crystal lattice. However, a significant disorder fraction remains even after 1000 °C and, in fact, the observed damage formation/evolution is similar to that for the Zn implants (Sec. III A) with preferential formation of extended defects. This conclusion is supported by the high resolution TEM results in Figs. 10(a) and 10(b) taken near the surface of the as-implanted and 800 °C annealed Ag samples, respectively. A high density of planar defects, such as stacking faults, is clearly visible in the disordered region of the as-implanted sample, while annealing leads predominantly to shrinkage in size of

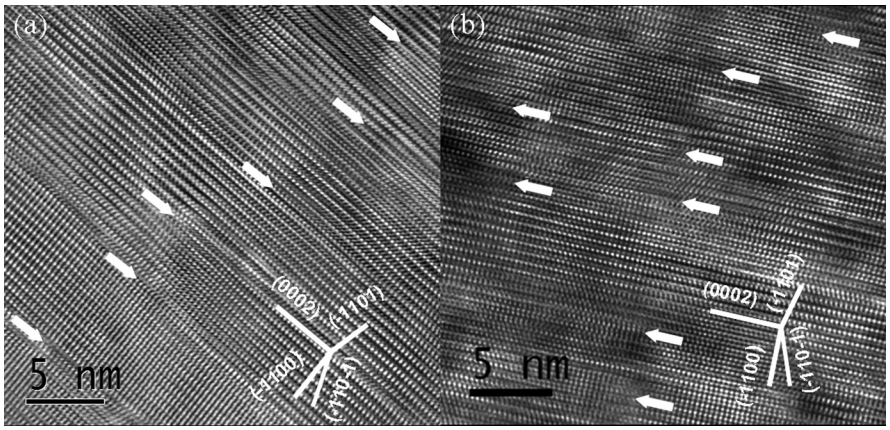

FIG. 10. High resolution TEM images of ZnO samples implanted with 500 keV Ag ions to 5×10^{15} cm^{-2} (a) before and (b) after annealing at 800 °C. The images are taken near the surface part of the damaged region along the ⟨11–20⟩ zone axis with different planes indicated.

the basal plane stacking faults. Indeed, the analysis of HRTEM images indicates that the average length of stacking faults decreases from ~15 nm to ~4 nm by the 800 °C annealing.

Implantation-induced formation of extended defects lying in the basal plane is typical for materials having wurtzite structure[44] and has been observed previously in ZnO,[5,8] although such a strong effect as for Ag is exceptional. The stark difference in damage formation/evolution between the Cd and Ag implanted samples indicates that presence of Ag is crucial for the enhanced concentration of planar defects. The exact role of the Ag atoms is, however, not clear but it can be suggested that Ag agglomerations occurs. Indeed, the large difference in ionic radii between Ag^{+} (0.102 nm) and Zn^{2+} (0.056 nm) and a relatively low Ag solid solubility enable efficient Ag clustering (especially at high Ag concentrations), as suggested by first principle calculations.[45] Such inclusions can induce a local strain in the crystal lattice and stimulate formation of stacking faults which, in their turn, act as efficient sinks for the generated point defects suppressing the formation of point defect clusters.

G. Implantation with heavy ions

Figs. 11(a) and 11(b) show RBS/C spectra of samples implanted with Au and Bi ions, respectively. Both samples display a similar damage evolution with temperature up to 800 °C as the Cd implanted ones (Fig. 9(a)). However, at 900 °C, a strong crystal recovery occurs in the Bi samples, while the Au sample remains almost unchanged. The strong recovery is accompanied by a pronounced out-diffusion of Bi through the surface resulting in ≈70% loss of the Bi content.

Also for these heavy elements, it is crucial to monitor their atomic position and the inset in Fig. 11(b) shows the fraction of implanted ions occupying substitutional sites as a function of annealing temperature.[46] As-implanted Au and Bi ions occupy preferentially nonsubstitutional (displaced) positions and the on-site Au(Bi) fraction increases with increasing temperature, reaching ~10–20% after 800 °C. In contrast, Cd ions exhibit a rather different behavior; despite a substitutional fraction of 35–40% already in the as-implanted state, the substitutional fraction of Cd increases drastically above 500 °C and reaches ~80% after 800 °C. However, in spite of the different behaviors of the Cd and Au(Bi) species, the damage evolution in samples implanted with these ions exhibits the same trend, suggesting a minor role of the dopant lattice site location on the annealing processes in these samples.

For Er (Fig. 12(a)), the damage displays high thermal stability and 800 °C annealing results only in a small crystal recovery around R_p, whilst the substitutional fraction of Er decreases from 45% in the as-implanted state to below the detection limit. Further annealing at 1050 °C leads to an

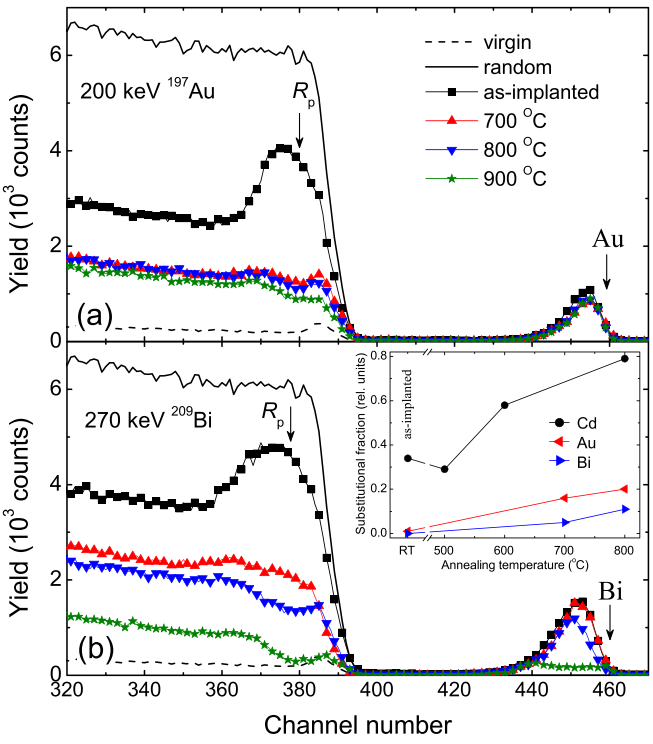

FIG. 11. RBS/C spectra (acquired with 170° detector geometry) of HT-ZnO implanted with (a) 200 keV $^{197}Au^{+}$ ions to 5×10^{15} cm^{-2} and (b) 270 keV $^{209}Bi^{+}$ ions to 1×10^{16} cm^{-2} before and after annealing as indicated in the legend (panel (a)). The channeling spectra of unprocessed (virgin) samples are shown for comparison by the dashed lines. The surface positions of implanted atoms are indicated by corresponding arrows, while the projected ranges of the implanted ions (R_p), predicted by TRIM code[25] simulations are depicted in the panels relative to the Zn depth scale. The inset in the panel (b) shows the fraction of implanted ions located at substitutional (non-scattering) sites as a function of annealing temperature for ZnO implanted with Cd, Au, and Bi.

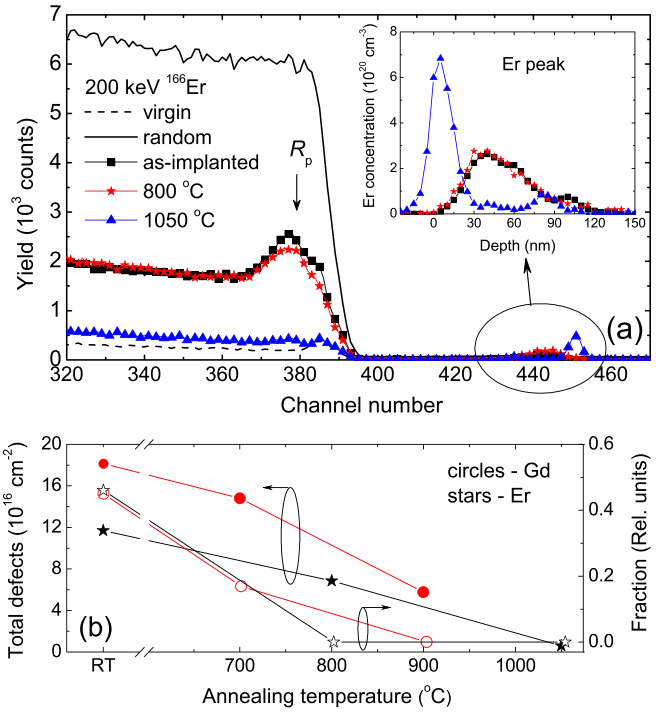

FIG. 12. (a) RBS/C spectra (acquired with 170° detector geometry) of HT-ZnO implanted with 200 keV $^{166}Er^+$ ions to 1.5×10^{15} cm^{-2} before and after annealing as indicated in the legend. The Er depth profiles calculated from RBS spectra are shown in the inset. The channeling spectrum of unprocessed (virgin) sample is shown for comparison by the dashed line. The projected range of the implanted ions (R_p), predicted by TRIM code[25] simulations, is depicted in the panel relative to the Zn depth scale. (b) The total amount of defects (closed symbols) and the substitutional fraction of implanted ions (open symbols) in ZnO implanted with Er and Gd ions (220 keV, 3.5×10^{15} cm^{-2}) as a function of annealing temperature.

almost complete damage removal accompanied by strong Er out-diffusion and segregation at the surface, as clearly unveiled by the data in the inset in Fig. 12(a) showing a shift of the Er peak to the surface. Note that the damage evolution in the Er implanted samples cannot be attributed to the low ion dose used in comparison with that of the other heavy implants (see the Table I for details). Indeed, it has been shown recently[47] that the characteristic annealing features are not a function of ion dose above a certain value and, for example, the defect evolution in Au implanted samples has a similar behavior with temperature irrespective of dose in the range of 3–30 DPA. Instead, the relatively high thermal stability of the damage in the Er samples compared with that for the other heavy implants is possibly due to formation/evolution of O-Er complexes, in analogy with that found by Alves *et al.*[48] for Er+O co-implanted GaN samples. Furthermore, it has been shown that the optically active center of Er in ZnO has the local structure similar to an ErO_6 complex, so that the local surrounding of optically active Er atom consists of six oxygen atoms forming an octahedron.[49] In addition, erbium oxide formation can play a role in defect formation for higher implanted doses.

Interestingly, Fig. 12(b) shows the total amount of defects (scattering centers) and substitutional (non-scattering) dopant fraction in samples implanted with Gd (Ref. 50) and Er ions as a function of annealing temperature. The disorder and the substitutional fraction exhibit identical behavior for both Gd and Er. In direct contrast, Murmu *et al.*[51] have reported almost complete lattice recovery in Gd implanted samples after 750 °C anneals performed in vacuum. Evidently, annealing in oxygen poor ambient, like vacuum, can lead to pronounced oxygen loss and dissociation of Gd-O complexes and, therefore, also reduce the thermal stability of ion-induced defects involving oxygen.

H. Role of implanted dose

In Secs. III A–III G, we have demonstrated a complex thermal behavior of ion-induced defects with the type of implanted species, using one dose for each species (except the N for which two doses were used). However, it is known that the amount of damage and/or its structure depend on the implanted dose and, this holds especially for heavy ions where the ion-induced disorder is characterized by an anomalous multipeak distribution.[5,28] Therefore, in this section, we investigate the thermal evolution of ion-induced disorder in samples implanted with Cd ions to "low" (5×10^{14} cm^{-2}), "medium" (2×10^{15} cm^{-2}), and "high" (5×10^{15} cm^{-2}) doses resulting in DPA values of 2.2, 8.8, and 22, respectively. Note that all these doses correspond to the third damage accumulation stage as mentioned in Sec. I. Fig. 13 shows the maximum relative disorder as a function of annealing temperature for the three different doses, and a non-trivial evolution with dose is revealed. All the samples have almost the same damage level after the first annealing stage (>500 °C), despite the large difference in the disorder in the as-implanted states. This indicates that the fast growing type-III damage accumulation stage (corresponding to the dose range of 1-20 DPA) is mainly due to point defects and small defect clusters, which require a relatively low

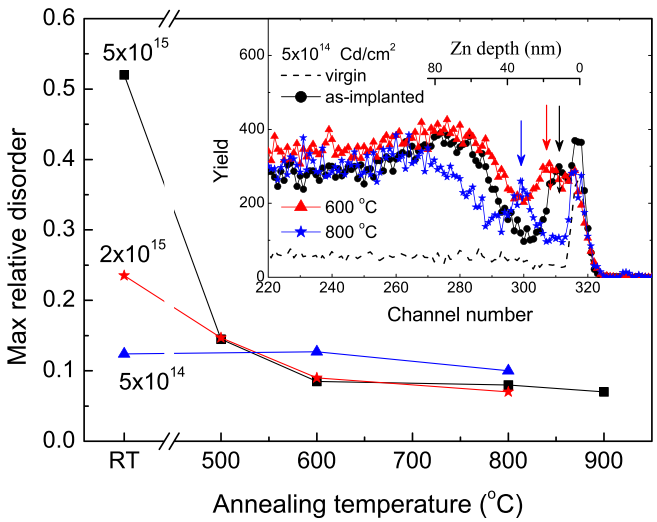

FIG. 13. Relative disorder on the Zn-sublattice as deduced from the maximum of the damage profiles in ZnO implanted with 250 keV $^{112}Cd^+$ ions to different doses as a function of annealing temperature. The inset shows RBS/C spectra (acquired with 100° detector geometry) of the samples implanted with Cd ions to 5×10^{14} cm^{-2} before and after annealing as indicated in the legend. The channeling spectrum of unprocessed (virgin) sample is shown for comparison by the dashed line. The positions of IP are indicated by the arrows in the inset (see the text for clarification).

temperature to disappear after heavy ions implants (irrespective of dose), as shown in Secs. III F and III G.

Interestingly, despite that the total amount of defects remains almost unchanged after annealing at least up to 800 °C in the low dose sample, the disorder depth distribution exhibits considerable evolution with increasing temperature. The inset in Fig. 13 shows RBS/C spectra of the low dose sample before and after annealing, and the as-implanted disorder profile displays an anomalous multipeak distribution with an intermediate defect peak (IP) between the more expected surface and bulk damage peaks. This additional peak is partly overlapping with the surface one and its formation is consistent with previous studies of damage accumulation in ZnO samples implanted with heavy or cluster ions creating dense collision cascades.[5,28] In contrast to medium and high dose implantations (Figs. 13 and 9), 600 °C annealing has only a small effect on the main defect peak in the low dose sample but IP shifts distinctly towards the bulk. Further annealing at 800 °C results in additional IP shift by ~20 nm and lowering of the defect concentration in the vicinity of IP. It should be noted that annealing of Cd samples at the temperatures higher than 1000 °C leads to the similar effects as observed for Bi (see Sec. III G), i.e., an efficient defect removal and a dramatic Cd loss via the surface (not shown).

The mechanisms of IP formation are not well understood; however, Myers *et al.*[52] have recently suggested that IP is related to the defect band at the interface between stoichiometric ZnO and the near-surface part of the sample which may have an altered composition due to O clustering or loss. The importance of O loss for the IP formation is indirectly supported by the results of Pereira *et al.*[53] who observed formation of a multipeak disorder distribution in Fe implanted samples already after 500 °C annealing in vacuum. Evidently, the movement of such an interface can be promoted by sample decomposition invoking O loss at the surface. Concurrently, the moving IP can act as a sink trapping/annihilating mobile point defects and, therefore, decrease the defect concentration in its vicinity.

IV. CONCLUSIONS

The defect evolution in ion implanted ZnO exhibits a complex behavior with annealing temperature and strongly depends on the implanted species and the associated defect formation. In particular, out-diffusion of the implanted species correlates with an efficient crystal recovery at relatively low temperatures. In contrast to light and medium mass ion implants, like B, O, and Zn, the damage produced by heavy implants (such as Cd, Au, and Bi) exhibits a distinct two-stage behavior involving annealing of point defects (or small defect clusters) and extended defects, respectively. These extended defects require significantly higher temperature to disappear and cannot be efficiently removed even at 900 °C. The strong effects of the implanted species on the damage evolution are especially pronounced for N, Ag, and Er. For Ag, the disorder is characterized by an enhanced concentration of extended defects having a second annealing stage at temperatures above 600 °C. For Er, the damage exhibits high thermal stability compared with that for other heavy ions and efficient crystal recovery occurs only at temperatures ≥1000 °C, accompanied by a pronounced Er out-diffusion and segregation at the surface. In contrast to other species, the damage in N implanted samples has an exceptionally high thermal stability and a significant amount of defects is present even after annealing at 1000 °C. Furthermore, for low N doses, a dramatic reverse annealing occurs, where the integral damage increases with temperature reaching a maximum after 650 °C. The influence of the implanted elements on the damage evolution is in most cases attributed to formation of complexes between the implanted species and O-related defects.

ACKNOWLEDGMENTS

Financial support from the Norwegian Research Council (FRINATEK program) is gratefully acknowledged.

[1]Ü. Özgür, Ya. I. Alivov, C. Liu, A. Teke, M. A. Reshchikov, S. Doğan, V. Avrutin, S.-J. Cho, and H. Morkoç, J. Appl. Phys. **98**, 041301 (2005).
[2]A. Janotti and C. G. Van de Walle, Rep. Prog. Phys. **72**, 126501 (2009).
[3]V. Avrutin, N. Izyumskaya, Ü. Özgür, D. J. Silversmith, and H. Morkoç, Proc. IEEE **98**, 1288 (2010).
[4]A. B. Djurišić and Y. H. Leung, Small **2**, 944 (2006).
[5]S. O. Kucheyev, J. S. Williams, C. Jagadish, J. Zou, C. Evans, A. J. Nelson, and A. V. Hamza, Phys. Rev. B **67**, 094115 (2003).
[6]A. Yu. Azarov, A. I. Titov, P. A. Karaseov, S. O. Kucheyev, A. Hallén, A. Yu. Kuznetsov, B. G. Svensson, and A. P. Pathak, Vacuum **84**, 1058 (2010).
[7]K. Lorenz, E. Alves, E. Wendler, O. Bilani, W. Wesch, and M. Hayes, Appl. Phys. Lett. **87**, 191904 (2005).
[8]G. Perillat-Merceroz, P. Gergaud, P. Marotel, S. Brochen, P.-H. Jouneau, and G. Feuillet, J. Appl. Phys. **109**, 023513 (2011).
[9]C. Ronning, P. X. Gao, Y. Ding, Z. L. Wang, and D. Schwen, Appl. Phys. Lett. **84**, 783 (2004).
[10]E. Rita, E. Alves, U. Wahl, J. G. Correia, T. Monteiro, M. J. Soares, A. Neves, and M. Peres, Nucl. Instrum. Methods Phys. Res., Sect. B **242**, 580 (2006).
[11]A. Yu. Azarov, A. I. Titov, and S. O. Kucheyev, J. Appl. Phys. **108**, 033505 (2010).
[12]S. Charnvanichborikarn, M. T. Myers, L. Shao, and S. O. Kucheyev, Scr. Mater. **67**, 205 (2012).
[13]M. A. Myers, M. T. Myers, M. J. General, J. H. Lee, L. Shao, and H. Wang, Appl. Phys. Lett. **101**, 112101 (2012).
[14]T. Monteiro, C. Boemare, M. J. Soares, E. Rita, and E. Alves, J. Appl. Phys. **93**, 8995 (2003).
[15]E. Sonder, R. A. Zhur, and R. E. Valiga, J. Appl. Phys. **64**, 1140 (1988).
[16]X. Ming, F. Lu, Z. Ji, M. Chen, J. Zhao, J. Yin, and Y. Ma, Nucl. Instrum. Methods Phys. Res., Sect. B **274**, 172 (2012).
[17]Z. Q. Chen, M. Maekawa, A. Kawasuso, S. Sakai, and H. Naramoto, J. Appl. Phys. **99**, 093507 (2006).
[18]T. M. Børseth, F. Tuomisto, J. S. Christensen, E. V. Monakhov, B. G. Svensson, and A. Yu. Kuznetsov, Phys. Rev. B **77**, 045204 (2008).
[19]R. Khanna, K. Ip, Y. W. Heo, D. P. Norton, S. J. Pearton, and F. Ren, Appl. Phys. Lett. **85**, 3468 (2004).
[20]A. Yu. Azarov, A. Hallén, X. L. Du, Z. L. Liu, B. G. Svensson, and A. Yu. Kuznetsov, Phys. Rev. B **84**, 014114 (2011).
[21]A. Yu. Azarov, E. Wendler, A. Yu. Kuznetsov, and B. G. Svensson, Appl. Phys. Lett. **104**, 052101 (2014).
[22]Quoted DPA values are the concentrations of ion-beam-generated lattice vacancies at the maximum of the nuclear energy loss profile (R_{pd}) calculated with TRIM code (Ref. 25) simulations and normalized to the atomic concentration of ZnO ($n_{at} = 8.3 \times 10^{22}$ atoms/cm^3). The effective threshold energies for atomic displacements were chosen of 34 and 44 eV for Zn and O sublattices, respectively (D. C. Look, G. C. Farlow, P. Reunchan, S. Limpijumnong, S. B. Zhang, and K. Nordlund, Phys. Rev. Lett. **95**, 225502 (2005)).

[23]A. Yu. Azarov, P. T. Neuvonen, K. E. Knutsen, L. Vines, B. G. Svensson, and A. Yu. Kuznetsov, Phys. Rev. Lett. **110**, 175503 (2013).
[24]P. A. Karaseov, A. Yu. Azarov, A. I. Titov, and S. O. Kucheyev, Semiconductor **43**, 691 (2009).
[25]J. F. Ziegler, J. P. Biersack, and U. Littmark, *The Stopping and Range of Ions in Solids* (Pergamon, Oxford, 1985), Vol. 1, p. 109.
[26]K. Schmid, Radiat. Eff. **17**, 201 (1973); R. S. Walker and D. A. Thompson, Nucl. Instrum. Methods **135**, 489 (1976).
[27]A. Turos, O. Meyer, L. Nowicki, J. Remmel, and M. Wielunski, Nucl. Instrum. Methods Phys. Res., Sect. B **85**, 448 (1994).
[28]A. Yu. Azarov, S. O. Kucheyev, A. I. Titov, and P. A. Karaseov, J. Appl. Phys. **102**, 083547 (2007).
[29]A. Turos, L. Nowicki, A. Stonert, K. Pagowska, J. Jagielski, and A. Muecklich, Nucl. Instrum. Methods Phys. Res., Sect. B **268**, 1718 (2010).
[30]P. Erhart and K. Albe, Appl. Phys. Lett. **88**, 201918 (2006).
[31]L. C. Kimerling, Solid-State Electron. **21**, 1391 (1978).
[32]A. Yu. Azarov, B. G. Svensson, and A. Yu. Kuznetsov, Appl. Phys. Lett. **101**, 222109 (2012).
[33]J. P. de Souza, H. Boudinov, and P. F. P. Fichtner, Appl. Phys. Lett. **64**, 3596 (1994).
[34]Note that low temperature experiments (15 K) have revealed roughly the same damage production rate normalized to DPA, for N ions as that for other medium mass and heavy elements.[7] However, a direct comparison of the data from Ref. 7 and present study is difficult due to the different implantation conditions used.
[35]O. Moutanabbir, B. Terreault, M. Chicoine, F. Schiettekatte, and P. J. Simpson, Phys. Rev. B **75**, 075201 (2007).
[36]Z. F. Di, Y. Q. Wang, M. Nastasi, and N. D. Theodore, Appl. Phys. Lett. **96**, 154103 (2010).
[37]N. Desrosiers, A. Giguère, B. Terreault, M. Chicoine, and F. Schiettekatte, Nucl. Instrum. Methods Phys. Res., Sect. B **266**, 1971 (2008).
[38]Note that despite RBS/C technique reveals primarily interstitial type defects, open volume defects like vacancies and vacancy clusters can induce local stress and contribute to the backscattering yield during RBS/C analysis.
[39]X. H. Li, H. Y. Xu, X. T. Zhang, Y. C. Liu, J. W. Sun, and Y. M. Lu, Appl. Phys. Lett. **95**, 191903 (2009).
[40]J. L. Lyons, A. Janotti, and C. G. Van de Walle, Appl. Phys. Lett. **95**, 252105 (2009).
[41]The NRA/C spectra were measured using 3.07 MeV He ions, so that the depth where the $^{16}O(\alpha, \alpha)\ ^{16}O$ resonance occurs roughly corresponds to ~70 nm, which is close to R_p of the N ions. Note that some difference in the damage levels on the Zn- and O-sublattices in Fig. 4 can primarily be attributed to poor depth resolution of NRA which is determined by the width of the resonance, and, secondly to different algorithms used for the calculation of relative disorder from RBS/C and NRA/C data.
[42]F. Tuomisto, C. Rauch, M. R. Wagner, A. Hoffmann, S. Eisermann, B. K. Meyer, L. Kilanski, M. C. Tarun, and M. D. McCluskey, J. Mater. Res. **28**, 1977 (2013).
[43]K. M. Johansen, A. Zubiaga, I. Makkonen, F. Tuomisto, P. T. Neuvonen, K. E. Knutsen, E. V. Monakhov, A. Yu. Kuznetsov, and B. G. Svensson, Phys. Rev. B **83**, 245208 (2011).
[44]C. M. Wang, W. Jiang, W. J. Weber, and L. E. Thomas, J. Mater. Res. **17**, 2945 (2002).
[45]O. Volnianska, P. Boguslawski, J. Kaczkowski, P. Jakubas, A. Jezierski, and E. Kaminska, Phys. Rev. B **80**, 245212 (2009).
[46]It should be noted that the shadowing effect was not taken into account for deduction of the substitutional fraction of the implanted species. This assumption may lead to some underestimation of the substitutional dopant fraction in heavily damaged crystals but is not critical to the conclusions made.
[47]A. Yu. Azarov, A. Hallén, B. G. Svensson, and A. Yu. Kuznetsov, J. Phys. D **45**, 235304 (2012).
[48]E. Alves, T. Monteiro, J. Soares, L. Santos, M. F. da Silva, J. C. Soares, W. Lojkowski, D. Kolesnikov, R. Vianden, and J. G. Correia, Mater. Sci. Eng. B **81**, 132 (2001).
[49]M. Ishii, S. Komuro, T. Morikawa, and Y. Aoyagi, J. Appl. Phys. **89**, 3679 (2001).
[50]A. Yu. Azarov, A. Audren, B. G. Svensson, A. Yu. Kuznetsov, and A. Hallén (unpublished).
[51]P. P. Murmu, R. J. Mendelsberg, J. Kennedy, D. A. Carder, B. J. Ruck, A. Markwitz, R. J. Reeves, P. Malar, and T. Osipowicz, J. Appl. Phys. **110**, 033534 (2011).
[52]M. T. Myers, S. Charnvanichborikarn, C. C. Wei, Z. P. Luo, A. Aitkaliyeva, L. Shao, and S. O. Kucheyev, Acta Mater. **60**, 6086 (2012).
[53]L. M. C. Pereira, U. Wahl, J. G. Correia, M. J. Van Bael, K. Temst, A. Vantomme, and J. P. Araújo, J. Phys.: Condens. Matter **25**, 416001 (2013).